ACS Energy LETTERS

http://pubs.acs.org/journal/aelccp

LETTER

Spherical Triboelectric Nanogenerator with Dense Point Contacts for Harvesting Multidirectional Water Wave and Vibration Energy

Zuqing Yuan, Chunfeng Wang, Jianguo Xi, Xun Han, Jing Li, Su-Ting Han,* Wenchao Gao,* and Caofeng Pan*

Cite This: *ACS Energy Lett.* 2021, 6, 2809−2816

Read Online

ACCESS | Metrics & More | Article Recommendations | Supporting Information

ABSTRACT: **Ocean wave energy is one of the most renewable energy sources. In this work, a spherical triboelectric nanogenerator (TENG) with dense point contacts can harvest water wave and vibration energy. Such spherical TENG consists of multiunits made of polyacrylate balls and thin fluorinated ethylene propylene films. The utilization of small polyacrylate balls enlarges the frequency of point contacts to enhance the contact efficiency and provides appropriate mechanical space to increase the volume power density. The spherical TENG transfer charges increased from about 21 nC to 820 nC with 1 to 15 units connected in parallel in the shell. The spherical TENG achieved a volume power density of 6.9 W m^{-3} at 0.8 Hz and 20.57 W m^{-3} at 5.9 Hz. Therefore, the spherical TENG provides a potential approach toward large-scale wave energy harvesting.**

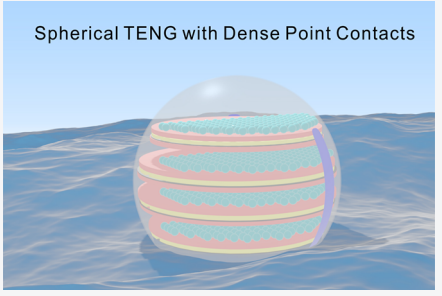

The sustainable development of human society promotes the exploration of energy in the new era.[1] The turbulent ocean wave energy is worth exploiting. Triboelectric nanogenerators (TENGs) have been a promising and efficient harvesting technology for converting the water wave energy into electrical power.[2,3] Compared to traditional electromagnetic generators, TENGs adapt to low-frequency motion and work based on the contact electrification and Maxwell's displacement current.[4−8] So far, TENGs have flexible, lightweight, and low-cost properties, exhibiting large potential applications, such as wearable devices, self-charged packages, and self-powered sensors.[9−18] Among them, spherical TENGs can waggle with the water wave to generate electrical output for the TENG.[19−21] However, the screening effect of the environmental ions has a negative influence on the charge transfer.[22−24] The electrostatic potential may attract ions, which decrease the charge transfer through the working circuit.[25] Furthermore, the surrounding electrodes have difficulty in increasing the working units.[26,27] Accordingly, a parallel-layer structure inside the shell can avoid the screening effect and obtain high performance for the spherical TENG.[28] The TENGs have been developed to harvest water wave energy from arbitrary directions based on the freestanding working mode.[29,30] These wave-driven TENGs could power batteries, sensors, and other self-powered devices.[31−35] However, how to arrange these freestanding polymers remains a challenge, because their volume, weight, and amount are the essential parameters.

In this work, a spherical TENG was designed and systematically investigated to harvest water wave energy. Such spherical TENG consisted of multiunits in a spherical shell. Each unit was made of polyacrylate (PA) balls and fluorinated ethylene propylene (FEP) films. The TENG units followed the working principle of freestanding mode.[36−40] The small PA balls increased the frequency of the point contacts with the FEP film to obtain a higher contact efficiency on the surface. The small-volume and lightweight properties of PA balls were also beneficial to achieve an optimized mechanical vibration. Besides, the spherical shell could contain more TENG units in parallel. The output charges increased with the increasing units. This structure improved the efficiency of harvesting water wave and vibration energy from arbitrary directions. Therefore, the spherical TENG provided an efficient approach toward large-scale wave energy harvesting.

Received: May 28, 2021
Accepted: July 12, 2021
Published: July 20, 2021

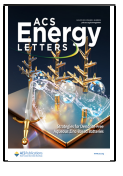

https://doi.org/10.1021/acsenergylett.1c01092
ACS Energy Lett. 2021, 6, 2809−2816

Concept and Structure of the Spherical TENG. The concept of the spherical TENG is schematically illustrated in Figure 1a. The water wave drives the orderly arranged spherical

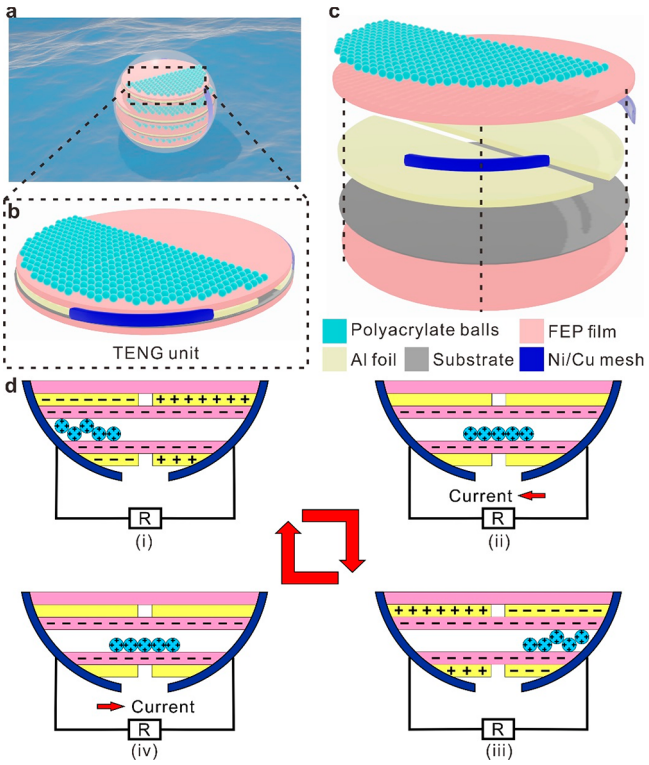

Figure 1. Schematic illustrations on the structure and working principle of the spherical TENG. (a) The schematic concept of the spherical TENG with dense point contacts. (b) A TENG unit inside the spherical shell. (c) The enlarged view of the TENG unit. (d) The freestanding working principle of the TENG follows steps (i) to (iv).

TENG, with freestanding PA balls continuously moving on the FEP films. In general, the motion or acceleration of the vibration-driven TENG acts indirectly on the inner structure to induce displacement current. The complex motion condition may not provide enough driving force for a fully contact-separation process. So minimizing the freestanding parts could be efficient, which will be demonstrated by this work. Another advantage is that the commercial PA balls are very cheap, which is about the 1000th of the price for commercial PTFE balls, and easy for large-scale production. The enlarged view of a single TENG unit is in Figure 1b. The small PA balls could obtain a higher contact efficiency than large objects and achieve greater volume power density. Simultaneously, the lightweight properties of PA balls increase the mechanical sensitivity to vibrations. The mass density of PA is 0.95 g cm^{-3}, lower than the 2.2 g cm^{-3} of PTFE. Moreover, a commercial PA ball in this work weighs about 17 mg, which is much lighter than a commercial PTFE ball. Then the spherical TENG could obtain a more significant acceleration under the same force.

The schematic illustration of a single TENG unit is in Figure 1c. The substrate paper is fixed on the inside shell to provide mechanical support to the unit. The PA balls are in the interspace between two triboelectric units and are always surrounded by FEP films. The interspace could contain no more than two layers of PA balls for dense stacking in the vertical direction, while the PA balls could move freely without apparent friction. The TENG units are connected in parallel by the Ni/Cu conducting mesh. The detailed fabrication process of the spherical TENG is described in the experimental method in Supporting Information.

Working Principle of the Spherical TENG. The working principle of the spherical TENG is in Figure 1d. Induced by water waves, the PA balls collide and contact with the FEP films inside the spherical shell. During the contact electrification, the PA balls gain positive surface charges, and the FEP films gain negative surface charges after initial vibration. The surface charges could maintain for a long time because they are trapped electrons in the potential well.[41,42] Figure 1d(i) displays the already-charged surfaces of both PA balls and FEP films. When PA balls move from the left to the right, the positive charges gradually induce negative electrons on the right electrode. The electrons flow back to the right electrode due to the electrostatic potential and generate the current in the circuit, as shown in Figure 1d(ii). Until the PA balls reach the right spherical shell, the current might exist. Figure 1d(iii) shows the gathered PA balls in the right corner. When the PA balls move back from right to left, the electrons gradually flow to the left electrode. The process generates a current in Figure 1d(iv) opposite to the one in Figure 1d(ii). The vibration excitations, such as water waves, will induce free electrons to flow between the two electrodes to produce alternating currents. Meanwhile, the spherical TENG transfers mechanical energy into electrical energy.

Structure Optimization of a Single TENG Unit. The amount of PA balls, double contact films, area of the triboelectric layer, and spacer gap of electrodes are the essential structural parameters in a single TENG unit. Figure 2a is a schematic illustration of these functional parts when the TENG unit works. At first, a specific TENG unit of 94 mm diameter was fixed to the spherical shell to study the structural parameters. The test utilized a layer of PA balls covering 50% area of the unit surface. A linear motor imposed reciprocating motion for the TENG unit. The initial linear motor setup was a reciprocating distance of 50 mm, acceleration of 20 ms^{-2}, and spare time of 200 ms. Other linear motor setup parameters in the following parts of this work could be found in Supporting Information Table S1. The optimum motion velocity was studied by recording the electrical output in real time in Figure 2b. The voltage, current, and transfer charges showed that the electrical output of the TENG unit reached saturation when the velocity was 1.0 ms^{-1}. So the velocity of 1.0 ms^{-1} was for the following discussion on the structural parameters of the TENG unit.

The amount of PA balls in the interspace was essential to reach the optimum output. The coverage ratio, defined as the area ratio that a layer of PA balls covers the TENG unit surface, could describe the amount. Figure 2c displays the performance comparison among the different coverage ratios. In the experiment, a half-open TENG unit with the ceiling empty was first utilized to study the coverage ratio. The results in Figure 2c displays that increasing free PA balls could enhance the output transfer charges. The transfer charges increased to 32 nC at the 100% coverage ratio. However, the half-open TENG had only a triboelectric FEP film layer, which limited the surface charge density. The other data columns were the results of containing the PA balls between double triboelectric FEP films. In this situation, the transfer charges reached 79 nC the at 60% coverage ratio. The double triboelectric films generated more surface charges than a single triboelectric film. However, the coverage ratio of over 60% decreased the transfer charges because the excessive PA balls jammed the freestanding motion.

https://doi.org/10.1021/acsenergylett.1c01092
ACS Energy Lett. 2021, 6, 2809−2816

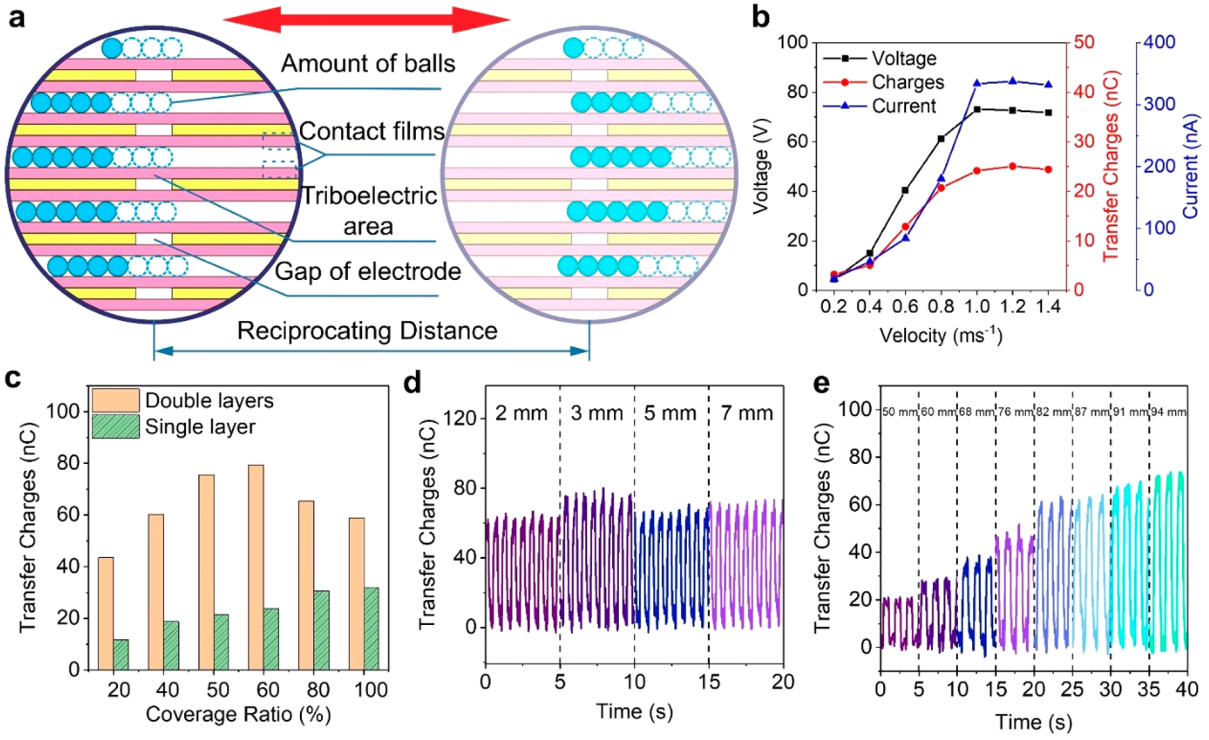

Figure 2. Structure optimization of a single TENG unit. (a) Schematic illustration of the essential structural parameters in a single TENG unit. (b) Velocity influenced the voltage, output current, and transfer charges of the TENG unit. (c) Transfer charges under different coverage ratios of PA balls for double and single triboelectric layers. (d) The electrode gap impacted the transfer charges. (e) The triboelectric area effectively tuned the transfer charges.

By balancing the unit weight and possible vibrating situation, the coverage ratio of 60% would be an optimum value.

The gap between the two electrodes could influence electrical performance. The gap width was tuned from 2 mm to 3 mm to 5 mm to 7 mm. Figure 2d displays that the 3 mm gap was the optimum width between the electrodes in the experiment. There might be two main factors. One was that the diameter of the PA balls was about 2.5 mm. The 3 mm gap was enough for the freestanding process of the PA balls. The other reason might be the functional working area and parasitic capacitance. In the spare time of the motion, the PA balls could heap up to the corner, while some PA balls left behind. The gap width of 5 mm and 7 mm reduced the working area of the unit. More PA balls were on the gap area in these situations, making minor contributions to the transfer charges. The last factor is the triboelectric layer area, which was regarded as the effective working area. Figure 2e compares the transfer charges in the increasing diameter of the TENG unit. The results show that the output transfer charges were directly proportional to the effective area under similar testing situations. On the other hand, the choice of ball materials should be considered in the optimization. Despite the wide choice of materials and potential modification, the PA balls remained to be a representative choice. The material choice was described in Supporting Information.

Performance of the TENG. The environmental factors were studied on the TENG output. The possible factors included wavelength, acceleration, frequency, and direction. The tested TENG unit had a diameter of 94 mm, a coverage ratio of 60%, an electrode gap of 3 mm, and double triboelectric layers. Moreover, the motion velocity was 1.0 ms^{-1}. Figure 3a shows the transfer charges of the TENG unit impacted by the simulated wavelength. The transfer charges were about 20 nC under the 10 mm wavelength and reached a saturation value of about 79 nC under the 50 mm wavelength. Under the minor wavelength, there was only a small mechanical force. When up to 50 mm wavelength, the PA balls could move to reach the other side to contribute to the transfer charges. As for the larger TENG units over 94 mm, increasing the wavelength may be necessary to guarantee the freestanding process.

To further discuss the influence of driving force, the TENG unit output was measured under different accelerations. The motion wavelength was fixed at 50 mm in this part. The electrical performance benefited from the acceleration, as shown in Figure 3b. With a change from 1 ms^{-2} to 5 ms^{-2}, the transfer charges increased from about 2.7 nC to 52 nC. It can be inferred that the possible activated acceleration was between 2 ms^{-2} and 5 ms^{-2}. Moreover, the transfer charges could reach about 94 nC at the 30 ms^{-2} acceleration, which increased by about 19% from the 20 ms^{-2} acceleration charges.

In the previous experiment, the linear motor provided enough spare time for the motion. The PA balls in the TENG unit moved sufficiently to the other side. However, the vibration frequency might change the motion of PA balls due to their lightweight and low friction force with FEP films. Figure 3c displays the output transfer charges under different frequencies. The experiment utilized the spare time to adjust the linear motion frequency in the experiment while keeping the acceleration at 20 ms^{-2} and velocity at 1.0 ms^{-1}. The output charges attained about 60 nC at 0.4 Hz. Due to the slow motion of PA balls, the signal drawback was associated with the electrostatic repulsive force among the PA balls. This phenomenon accompanied a small and reversed current peak. Moreover, the output transfer charges increased to 79 nC at 1.2

https://doi.org/10.1021/acsenergylett.1c01092
ACS Energy Lett. 2021, 6, 2809−2816

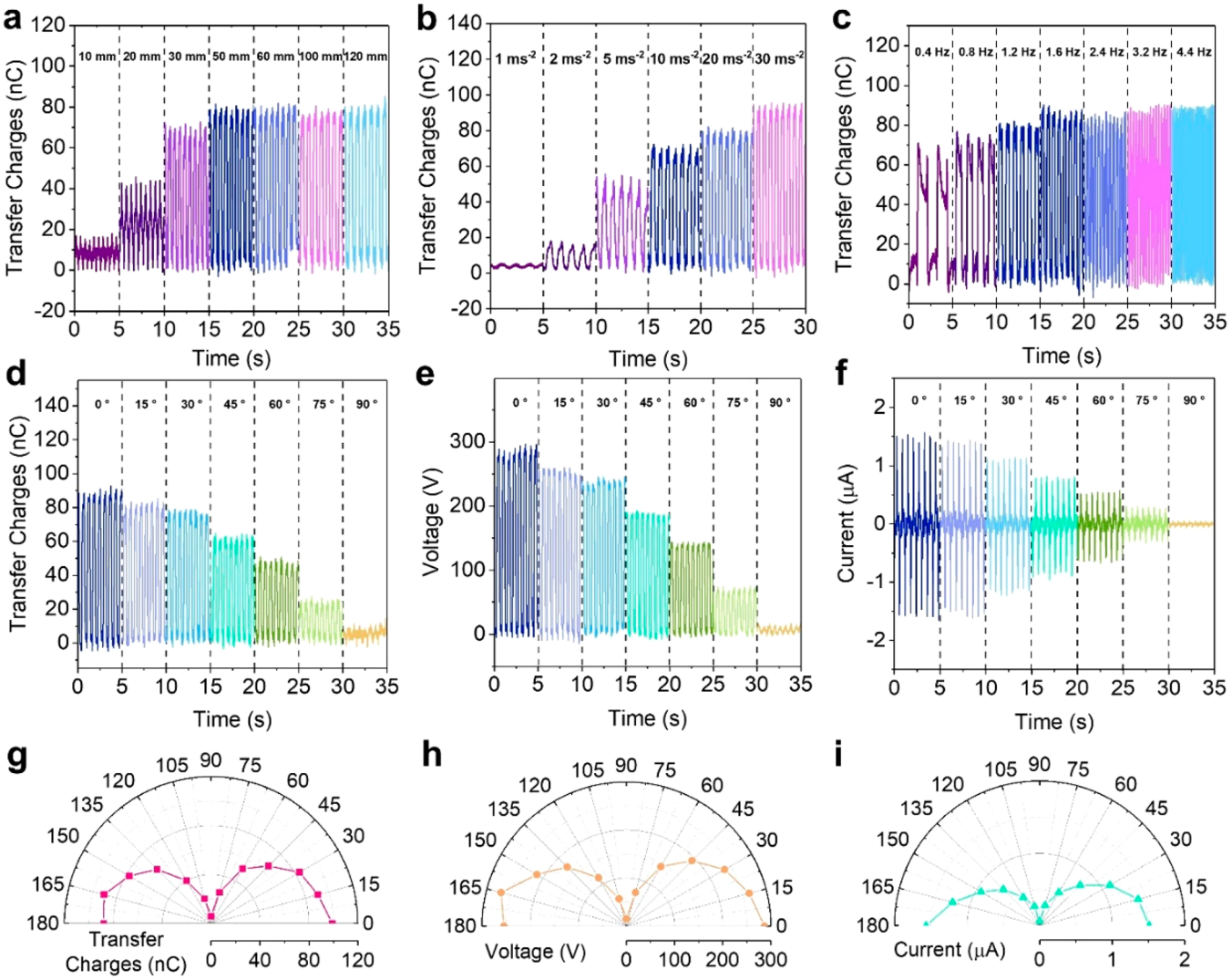

Figure 3. Electrical performance of the single TENG unit with different environmental factors. (a–c) The influence of wavelength (a), acceleration (b), and frequency (c) on the output transfer charges. (d–f) The results of the directions on the electrical performance of the single TENG unit, including transfer charges (d), open-circuit voltage (e), and short-circuit current (f). (g–i) The directional map of the transfer charges (g), voltage (h), and current (i) from 0 to 180°.

Hz and 88 nC at 4.4 Hz. The higher frequency achieved relatively stable transfer charges because the rapid motion avoided the drawback to a certain extent. The results show that the TENG unit could work at a wide range of frequencies from 0.1 to 5 Hz and realize potential applications to harvest mechanical energy, including the wind waves.

Harvesting vibration energy from arbitrary directions was also investigated for the TENG unit. The direction was defined as the intersection angle between the direction of electrodes and the vibration motion. Figure 3d–f show the measured transfer charges, open-circuit voltage, and short-circuit current with the intersection angle from 0 to 90°. The output transfer charges were different among the directions. From Figure 3d, the charges of 0° direction attained the highest values than others because the PA balls completely moved from one electrode to the other. On the other hand, 90° direction obtained the least output signals, which the PA balls mostly moved on a single electrode, leading to little charge transferring through the external circuits. The open-circuit voltage and short-circuit current in Figure 3e and f also reflected the changes due to the directions. Figure 3g–i show the directional map of the transfer charges, voltage, and current from 0 to 180°. And the state from 0 to 90° was similar to the state from 90 to 180°. The detailed results of the 0 and 180° directions were in Supporting Information Figure S3. The TENG unit could harvest wave energy from arbitrary directions, preferring the directions that provided enough movement for the PA balls to separate from one electrode to the other. From the results, the 0° direction had the most considerable influence on the output performance of the device. However, the output was reduced to the minimum value in the 90° direction.

Multiunits are inserted into the spherical shell to improve the volume power density of the whole spherical TENG, as shown in Figure 4a. When water waves drove the spherical TENG, all the units could harvest wave energy at the same time and work more effectively. The schematic illustration on the equivalent circuit of the working spherical TENG is in Figure 4b. The units are connected in parallel and rectified to power the external electronics.

The TENG units were built up from one layer to eight layers until occupying half the spherical shell. The diameters of the layers were 50 mm, 65 mm, 75 mm, 82 mm, 88 mm, 92 mm, 95

https://doi.org/10.1021/acsenergylett.1c01092
ACS Energy Lett. 2021, 6, 2809–2816

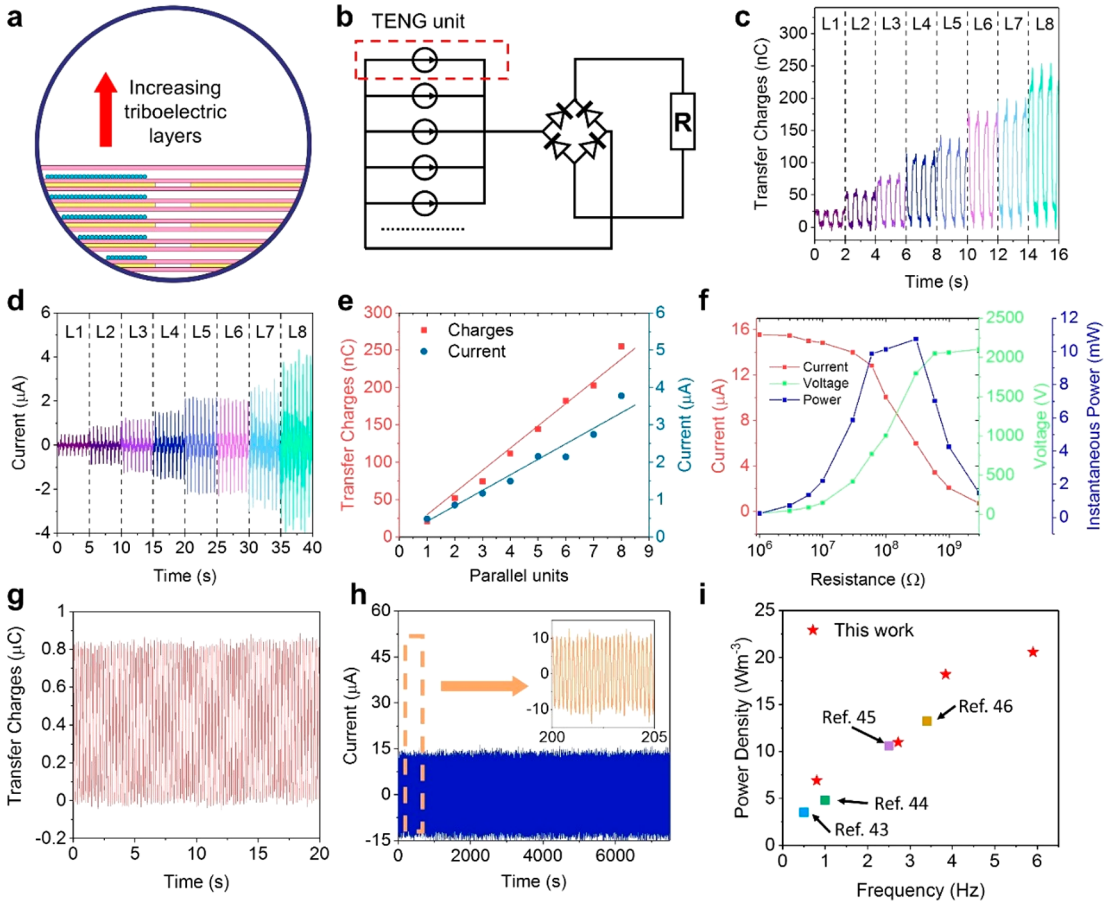

Figure 4. Electrical performance of the spherical TENG. (a) Schematic illustration on the TENG units inside the spherical shell. (b) The equivalent circuit of the TENG units connected in parallel and rectified to power the external load. (c, d) The transfer charges and current increased with layers. (e) The transfer charges and current were nearly linearly proportional to the number of units. (f) The instantaneous power of the spherical TENG varied with external resistance in series under 5.9 Hz vibration. (g) The transfer charges under 5.9 Hz vibration. (h) The 2 h test for output current of the spherical TENG at 4.4 Hz demonstrates its stability. (i) Comparison of the power density of the present spherical TENG, the sea snake TENG,[43] the multilayer and contact-separation spherical TENG,[44] the tower-like TENG,[45] and air-driven membrane structure TENG.[46]

mm, and 96 mm. Once adding a new layer, the electrical performance of the spherical TENG was measured. Figure 4c shows that the transfer charges increased from about 21 nC with one layer to 254 nC with eight layers. However, compared to the experimental results of individual layers in Figure 2e, the cumulative increase due to the additional layer was less than expected. For details, the transfer charges from layer 3 were about 22 nC in Figure 4c, but a similar TENG unit of 76 mm could output about 45 nC in Figure 2e. The difference was attributed to the charge redistribution in the multilayer electrodes and parasitic capacitance. A similar phenomenon was for the open-circuit voltage. Figure 4d shows that the short-circuit current increased from 0.47 to 3.8 μA with eight layers. To further illustrate the electrical performance, the output charges and current from the units were concluded in Figure 4e. The transfer charges and current were nearly proportional to the number of units.

The further experiment measured the electrical performance of the whole spherical TENG. The spherical TENG consisted of 15 units in parallel and evenly distributed inside the spherical shell. The fabricated spherical TENG weighed about 209 g. The current of the spherical TENG was tested with different resistances, as shown in Figure 4f. The voltage was obtained by multiplying the current and resistance, and the instantaneous power was obtained by multiplying the current and voltage. The spherical TENG was motivated by the linear motor with the 50 mm reciprocating distance, 30 ms^{-2} acceleration, 1.0 ms^{-1} velocity, and 0 ms spare time. At first, the tested current was about 15.5 μA at the 1 MΩ. The calculated voltage could reach about 2103 V at the 3 GΩ resistance. Moreover, the maximum instantaneous power reached about 10.7 mW at 5.9 Hz, when the resistance equals the internal 300 MΩ. There might be more extensive power in practical because the freestanding design could output the current with a longer duration than the vertical contact-separation process. Figure 4g shows the transfer charges of the whole spherical TENG could achieve about 820 nC at 5.9 Hz. A low-frequency test under 0.8 Hz for the spherical TENG was also carried out, as shown in Supporting Information Figure S4. The cycling test of output current was in Figure 4h. The spherical TENG worked under 4.4 Hz over 2 h, achieving about 10 μA for over 30000 cycles. The enlarged views of the current curve were in the insets. So the spherical TENG could work stably for both low and high frequency, which was appropriate for harvesting the wind-wave energy and other vibrations.

Figure 4i shows the power density of the spherical TENG increased by the frequency from 0.8 to 5.9 Hz. Compared with the previously reported results, the spherical TENG in this work achieved 6.9 W m^{-3} at 0.8 Hz, 10.9 W m^{-3} at 2.7 Hz, 18.1 W m^{-3}

https://doi.org/10.1021/acsenergylett.1c01092
ACS Energy Lett. 2021, 6, 2809−2816

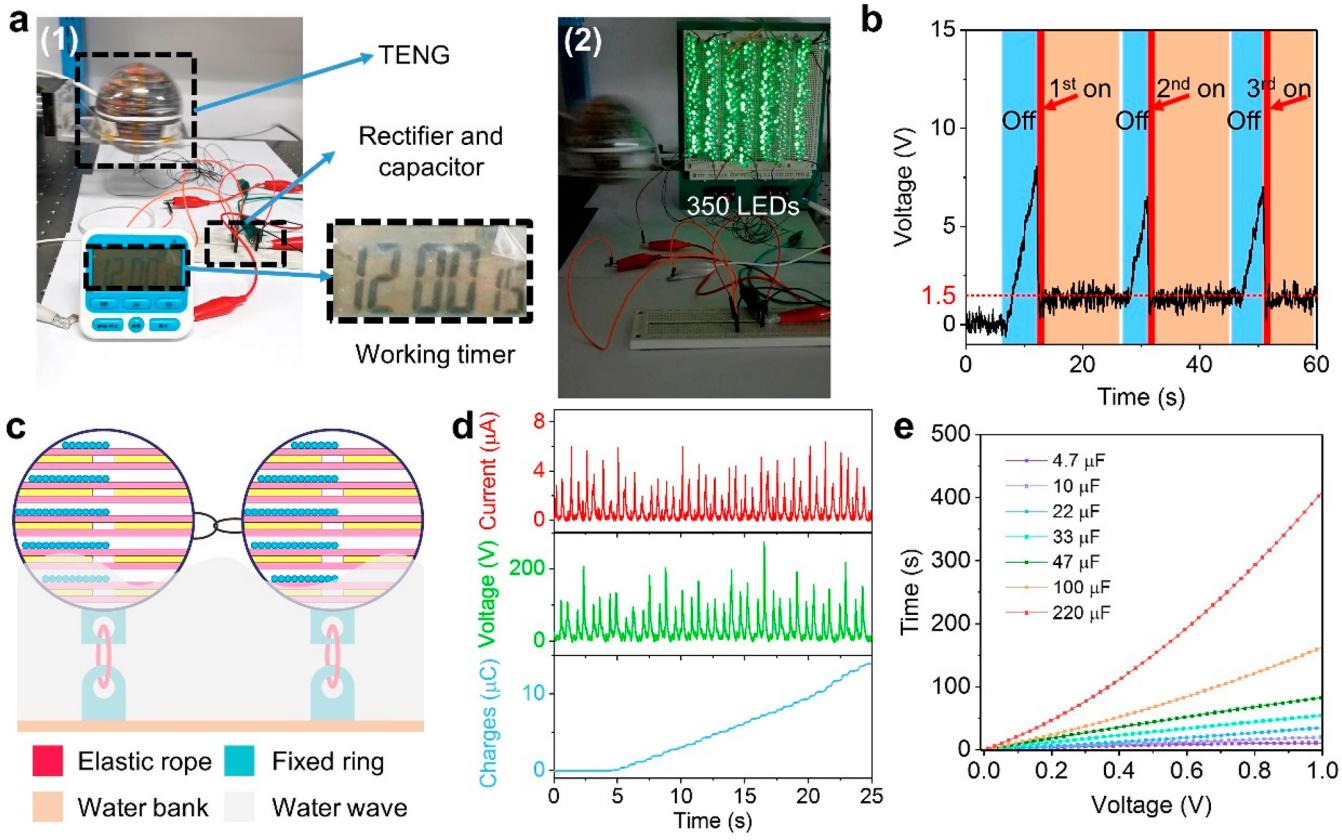

Figure 5. Spherical TENG harvested mechanical energy from the vibration and water wave. (a) The photos of powering a timer and LEDs by the TENG. (b) The voltage curve of the 4.7 μF capacitor to power the timer during three on−off switches. (c) The schematic setup of the spherical TENGs to harvest water energy. (d) The voltage, current, and charge of the two spherical TENGs with rectifiers. The resistance load for voltage was 100 MΩ. (e) The time cost to 1 V for the different capacitors charged by the spherical TENGs under water waves.

at 3.8 Hz, and 20.5 W m^{-3} at 5.9 Hz. The results show a significant advance in the power density that dense point contacts could provide a more efficient contact than the thin film or bulk structure. So minimizing the freestanding parts could be efficient, which was demonstrated by this work. Simultaneously, the efficiency could further increase by building a cylinder and uniform multilayered structure to enclose more and larger TENG units in a shell.

Demonstration to Harvest Vibration Energy. The spherical TENG could continuously power a timer in Figure 5a(1) and light 350 green LEDs in Figure 5a(2). The current pulses from a spherical TENG were first modulated by a rectifier and a 4.7 μF capacitor to power other devices. The videos in the Supporting Information Video S1 and S2 could demonstrate the working. While powering the timer, the voltage of the capacitor was monitored by the electrometer in real time. The results in Figure 5b show the three switches of the timer between the off-state and on-state. The capacitor voltage rapidly increased when switched off but decreased sharply with the switch on due to the consumption of the timer. The voltage was maintained at a slightly lower level than 1.5 V and could continuously supply the timer.

In the demonstration to harvest water wave energy, two spherical TENGs were connected in one block to harvest water wave energy in a water tank. The fixed rings were prepared at the bottom of the spherical shell and the water bank in advance. Before pouring in the water, the rings were tied to each other by elastic ropes of the same length. Then the water leveled up to about 15 cm that could float the spherical TENGs. Based on this setup, the TENGs could vibrate with the water wave, as shown in Figure 5c. Unstable water waves with multi frequencies and amplitudes were generated by a push plate to drive the spherical TENGs. Figure 5d shows the voltage, current, and charge of the two spherical TENGs in parallel. Each spherical TENG was equipped with a rectifier for the direct current. Under the unstable wave, the voltage with the load of 100 MΩ resistance in the circuit could remain over 100 V for a water wave. The current could be over 3 μA, and the charges reached the magnitude of μC in a water wave. The wave-driving process of the spherical TENGs was displayed in Supporting Information Video S3. The current peaks could be influenced by controlled waves frequencies, as displayed in Supporting Information Figure S5. Then, the wave-driving spherical TENGs were applied to power energy storage devices. The rectifier and various capacitors were utilized to investigate the electrical performance of the TENGs. The charging time cost was recorded until the voltage was 1 V. The spherical TENGs charged the 4.7 μF capacitor to 1 V within 11 s. When charging larger capacitors, the time cost increased, as shown in Figure 5e. The voltage of the 220 μF capacitor reached 1 V in 410 s, and as for the 100 μF capacitor, the time was about 161 s. The above measurements provided a credible demonstration for long-term and large-area harvesting water wave energy. Therefore, the spherical TENGs provide a potential approach toward harvesting blue energy as sustainable power networks.

In summary, this work provides a TENG based on dense point contacts to harvest vibration and water wave energy. The TENG consists of multiunits with small PA balls and FEP films. There is

https://doi.org/10.1021/acsenergylett.1c01092
ACS Energy Lett. 2021, 6, 2809−2816

dense contact electrification between the PA balls and FEP films. The TENG works on the freestanding mode and can effectively convert vibration energy into electrical energy. The small and lightweight PA balls provide the fitness to various frequencies, which the experimental results have demonstrated from 0 to 5.9 Hz. Moreover, the volume power density of the spherical TENG can reach 6.9 W m^{-3} at 0.8 Hz and 20.5 W m^{-3} at 5.9 Hz. The output charges are enhanced up to 820 nC with 15 TENG units. The spherical shell provides mechanical and electrical protection from the external environment, which is essential for stable performance under long-cycle tests. Furthermore, the whole spherical TENG could light 350 LEDs and power a timer. In the water bank, the spherical TENGs can charge the various capacitors in minutes. This is a significant work that improved the internal structure of the spherical TENG to increase its energy conversion efficiency. Some analysis of hydrodynamics and structural mechanics will be studied in future work, which are the key factors for the ultimate realization of blue energy.

■ ASSOCIATED CONTENT

Supporting Information

The Supporting Information is available free of charge at https://pubs.acs.org/doi/10.1021/acsenergylett.1c01092.

Experimental procedures, schematic illustration of manufacture, a table of linear motor setup, figures showing the choice of ball materials for their weight and electrical performance, directions of 0 to 180° on the electrical performance, electrical outputs of the spherical TENG under low-frequency vibration and water wave (PDF)

Powering a timer by a spherical TENG (MP4)

Lighting 350 LEDs by a spherical TENG (MP4)

Wave-driving process of the spherical TENGs (MP4)

■ AUTHOR INFORMATION

Corresponding Authors

Su-Ting Han − *Institute of Microscale Optoelectronics, Shenzhen University, Shenzhen 518060, China;* orcid.org/0000-0003-3392-7569; Email: sutinghan@szu.edu.cn

Wenchao Gao − *Department of Civil Engineering, Monash University, Clayton 3800, Australia*; Email: wenchao.gao1@monash.edu

Caofeng Pan − *CAS Center for Excellence in Nanoscience, Beijing Key Laboratory of Micro-nano Energy and Sensor, Beijing Institute of Nanoenergy and Nanosystems, Chinese Academy of Sciences, Beijing 100083, P. R. China; School of Nanoscience and Technology, University of Chinese Academy of Sciences, Beijing 100049, P. R. China;* orcid.org/0000-0001-6327-9692; Email: cfpan@binn.cas.cn

Authors

Zuqing Yuan − *Institute of Microscale Optoelectronics, Shenzhen University, Shenzhen 518060, China;* orcid.org/0000-0003-3988-0618

Chunfeng Wang − *Institute of Microscale Optoelectronics, Shenzhen University, Shenzhen 518060, China; CAS Center for Excellence in Nanoscience, Beijing Key Laboratory of Micro-nano Energy and Sensor, Beijing Institute of Nanoenergy and Nanosystems, Chinese Academy of Sciences, Beijing 100083, P. R. China*

Jianguo Xi − *CAS Center for Excellence in Nanoscience, Beijing Key Laboratory of Micro-nano Energy and Sensor, Beijing Institute of Nanoenergy and Nanosystems, Chinese Academy of Sciences, Beijing 100083, P. R. China*

Xun Han − *Institute of Microscale Optoelectronics, Shenzhen University, Shenzhen 518060, China; CAS Center for Excellence in Nanoscience, Beijing Key Laboratory of Micro-nano Energy and Sensor, Beijing Institute of Nanoenergy and Nanosystems, Chinese Academy of Sciences, Beijing 100083, P. R. China*

Jing Li − *CAS Center for Excellence in Nanoscience, Beijing Key Laboratory of Micro-nano Energy and Sensor, Beijing Institute of Nanoenergy and Nanosystems, Chinese Academy of Sciences, Beijing 100083, P. R. China*

Complete contact information is available at: https://pubs.acs.org/10.1021/acsenergylett.1c01092

Notes

The authors declare no competing financial interest.

■ ACKNOWLEDGMENTS

The authors thank the support of National Natural Science Foundation of China (No. U20A20166, 61675027, 61805015 and 61804011), national key R & D project from Minister of Science and Technology, China (2016YFA0202703), Natural Science Foundation of Beijing Municipality (Z180011), Shenzhen Science and Technology Program (Grant No. KQTD20170810105439418), and the Fundamental Research Funds for the Central Universities.

■ REFERENCES

(1) Wu, C.; Wang, A. C.; Ding, W.; Guo, H.; Wang, Z. L. Triboelectric Nanogenerator: A Foundation of the Energy for the New Era. *Adv. Energy Mater.* **2019**, *9* (1), 1802906.

(2) Wang, Z. L. Catch wave power in floating nets. *Nature* **2017**, *542* (7640), 159−160.

(3) Painuly, J. P. Barriers to renewable energy penetration; a framework for analysis. *Renewable Energy* **2001**, *24* (1), 73−89.

(4) Zi, Y.; Guo, H.; Wen, Z.; Yeh, M.-H.; Hu, C.; Wang, Z. L. Harvesting Low-Frequency (<5 Hz) Irregular Mechanical Energy: A Possible Killer Application of Triboelectric Nanogenerator. *ACS Nano* **2016**, *10* (4), 4797−4805.

(5) Li, S.; Zhou, Y.; Zi, Y.; Zhang, G.; Wang, Z. L. Excluding contact electrification in surface potential measurement using kelvin probe force microscopy. *ACS Nano* **2016**, *10* (2), 2528−2535.

(6) Wang, Z. L. On the first principle theory of nanogenerators from Maxwell's equations. *Nano Energy* **2020**, *68*, 104272.

(7) Wang, Z. L. On Maxwell's displacement current for energy and sensors: the origin of nanogenerators. *Mater. Today* **2017**, *20* (2), 74−82.

(8) Bouendeu, E.; Greiner, A.; Smith, P. J.; Korvink, J. G. A Low-Cost Electromagnetic Generator for Vibration Energy Harvesting. *IEEE Sens. J.* **2011**, *11* (1), 107−113.

(9) Liu, G.; Xiao, L.; Chen, C.; Liu, W.; Pu, X.; Wu, Z.; Hu, C.; Wang, Z. L. Power cables for triboelectric nanogenerator networks for large-scale blue energy harvesting. *Nano Energy* **2020**, *75*, 104975.

(10) Khan, U.; Kim, S.-W. Triboelectric Nanogenerators for Blue Energy Harvesting. *ACS Nano* **2016**, *10* (7), 6429−6432.

(11) Huang, L.-b.; Xu, W.; Bai, G.; Wong, M.-C.; Yang, Z.; Hao, J. Wind energy and blue energy harvesting based on magnetic-assisted noncontact triboelectric nanogenerator. *Nano Energy* **2016**, *30*, 36−42.

(12) Shao, H.; Wen, Z.; Cheng, P.; Sun, N.; Shen, Q.; Zhou, C.; Peng, M.; Yang, Y.; Xie, X.; Sun, X. Multifunctional power unit by hybridizing contact-separate triboelectric nanogenerator, electromagnetic generator and solar cell for harvesting blue energy. *Nano Energy* **2017**, *39*, 608−615.

(13) Xia, K.; Fu, J.; Xu, Z. Multiple-Frequency High-Output Triboelectric Nanogenerator Based on a Water Balloon for All-Weather

Water Wave Energy Harvesting. *Adv. Energy Mater.* **2020**, *10* (28), 2000426.
(14) Liu, Y.; Wang, L.; Zhao, L.; Yu, X.; Zi, Y. Recent progress on flexible nanogenerators toward self-powered systems. *InfoMat* **2020**, *2* (2), 318−340.
(15) Ma, C.; Gao, S.; Gao, X.; Wu, M.; Wang, R.; Wang, Y.; Tang, Z.; Fan, F.; Wu, W.; Wan, H.; Wu, W. Chitosan biopolymer-derived self-powered triboelectric sensor with optimized performance through molecular surface engineering and data-driven learning. *InfoMat* **2019**, *1* (1), 116−125.
(16) Tang, Y.; Li, X.; Lv, H.; Wang, W.; Zhi, C.; Li, H. Integration designs toward new-generation wearable energy supply-sensor systems for real-time health monitoring: A minireview. *InfoMat* **2020**, *2* (6), 1109−1130.
(17) Pu, K.-C.; Zhang, X.; Qu, X.-L.; Hu, J.-J.; Li, H.-W.; Gao, M.-X.; Pan, H.-G.; Liu, Y.-F. Recently developed strategies to restrain dendrite growth of Li metal anodes for rechargeable batteries. *Rare Met.* **2020**, *39* (6), 616−635.
(18) Liu, Y.; Bao, R.; Tao, J.; Li, J.; Dong, M.; Pan, C. Recent progress in tactile sensors and their applications in intelligent systems. *Sci. Bull.* **2020**, *65* (1), 70−88.
(19) Cheng, P.; Guo, H.; Wen, Z.; Zhang, C.; Yin, X.; Li, X.; Liu, D.; Song, W.; Sun, X.; Wang, J. Largely enhanced triboelectric nanogenerator for efficient harvesting of water wave energy by soft contacted structure. *Nano Energy* **2019**, *57*, 432−439.
(20) Xu, L.; Jiang, T.; Lin, P.; Shao, J. J.; He, C.; Zhong, W.; Chen, X. Y.; Wang, Z. L. Coupled triboelectric nanogenerator networks for efficient water wave energy harvesting. *ACS Nano* **2018**, *12* (2), 1849−1858.
(21) Fan, X.; Liu, X.; Hu, W.; Zhong, C.; Lu, J. Advances in the development of power supplies for the Internet of Everything. *InfoMat* **2019**, *1* (2), 130−139.
(22) Pan, C.; Dong, L.; Zhu, G.; Niu, S.; Yu, R.; Yang, Q.; Liu, Y.; Wang, Z. L. High-resolution electroluminescent imaging of pressure distribution using a piezoelectric nanowire LED array. *Nat. Photonics* **2013**, *7* (9), 752−758.
(23) Pan, C.; Zhai, J.; Wang, Z. L. Piezotronics and Piezo-phototronics of Third Generation Semiconductor Nanowires. *Chem. Rev.* **2019**, *119* (15), 9303−9359.
(24) Hu, G.; Zhou, R.; Yu, R.; Dong, L.; Pan, C.; Wang, Z. L. Piezotronic effect enhanced Schottky-contact ZnO micro/nanowire humidity sensors. *Nano Res.* **2014**, *7* (7), 1083−1091.
(25) Lin, S.; Xu, L.; Chi Wang, A.; Wang, Z. L. Quantifying electron-transfer in liquid-solid contact electrification and the formation of electric double-layer. *Nat. Commun.* **2020**, *11* (1), 399.
(26) Liu, W.; Xu, L.; Bu, T.; Yang, H.; Liu, G.; Li, W.; Pang, Y.; Hu, C.; Zhang, C.; Cheng, T. Torus structured triboelectric nanogenerator array for water wave energy harvesting. *Nano Energy* **2019**, *58*, 499−507.
(27) Du, W.; Han, X.; Lin, L.; Chen, M.; Li, X.; Pan, C.; Wang, Z. L. A Three Dimensional Multi-Layered Sliding Triboelectric Nanogenerator. *Adv. Energy Mater.* **2014**, *4* (11), 1301592.
(28) Wu, Z.; Guo, H.; Ding, W.; Wang, Y.-C.; Zhang, L.; Wang, Z. L. A hybridized triboelectric−electromagnetic water wave energy harvester based on a magnetic sphere. *ACS Nano* **2019**, *13* (2), 2349−2356.
(29) Rodrigues, C.; Nunes, D.; Clemente, D.; Mathias, N.; Correia, J. M.; Rosa-Santos, P.; Taveira-Pinto, F.; Morais, T.; Pereira, A.; Ventura, J. Emerging triboelectric nanogenerators for ocean wave energy harvesting: state of the art and future perspectives. *Energy Environ. Sci.* **2020**, *13* (9), 2657−2683.
(30) Kim, D. Y.; Kim, H. S.; Kong, D. S.; Choi, M.; Kim, H. B.; Lee, J.-H.; Murillo, G.; Lee, M.; Kim, S. S.; Jung, J. H. Floating buoy-based triboelectric nanogenerator for an effective vibrational energy harvesting from irregular and random water waves in wild sea. *Nano Energy* **2018**, *45*, 247−254.
(31) Zuo, S.-L.; Chen, P.; Pan, C.-F. Mechanism of magnetic field-modulated luminescence from lanthanide ions in inorganic crystal: a review. *Rare Met.* **2020**, *39* (10), 1113−1126.
(32) Wang, X.; Zhang, H.; Yu, R.; Dong, L.; Peng, D.; Zhang, A.; Zhang, Y.; Liu, H.; Pan, C.; Wang, Z. L. Dynamic Pressure Mapping of Personalized Handwriting by a Flexible Sensor Matrix Based on the Mechanoluminescence Process. *Adv. Mater.* **2015**, *27* (14), 2324−2331.
(33) Wang, C.; Pan, C.; Wang, Z. Electronic Skin for Closed-Loop Systems. *ACS Nano* **2019**, *13* (11), 12287−12293.
(34) Sun, J. M.; Pu, X.; Jiang, C. Y.; Du, C. H.; Liu, M. M.; Zhang, Y.; Liu, Z. T.; Zhai, J. Y.; Hu, W. G.; Wang, Z. L. Self-powered electrochromic devices with tunable infrared intensity. *Sci. Bull.* **2018**, *63* (12), 795−801.
(35) Liu, J.; Zhang, Z.; Qiao, S.; Fu, G.; Wang, S.; Pan, C. Lateral bipolar photoresistance effect in the CIGS heterojunction and its application in position sensitive detector and memory device. *Sci. Bull.* **2020**, *65* (6), 477−485.
(36) Paosangthong, W.; Wagih, M.; Torah, R.; Beeby, S. Textile-based triboelectric nanogenerator with alternating positive and negative freestanding grating structure. *Nano Energy* **2019**, *66*, 104148.
(37) Ren, X.; Fan, H.; Wang, C.; Ma, J.; Li, H.; Zhang, M.; Lei, S.; Wang, W. Wind energy harvester based on coaxial rotatory freestanding triboelectric nanogenerators for self-powered water splitting. *Nano Energy* **2018**, *50*, 562−570.
(38) Zhang, N.; Qin, C.; Feng, T.; Li, J.; Yang, Z.; Sun, X.; Liang, E.; Mao, Y.; Wang, X. Non-contact cylindrical rotating triboelectric nanogenerator for harvesting kinetic energy from hydraulics. *Nano Res.* **2020**, *13* (7), 1903−1907.
(39) Jiang, D.; Ouyang, H.; Shi, B.; Zou, Y.; Tan, P.; Qu, X.; Chao, S.; Xi, Y.; Zhao, C.; Fan, Y.; Li, Z. A wearable noncontact free-rotating hybrid nanogenerator for self-powered electronics. *InfoMat* **2020**, *2* (6), 1191−1200.
(40) Liu, B.-H.; Xie, G.-Z.; Li, C.-Z.; Wang, S.; Yuan, Z.; Duan, Z.-H.; Jiang, Y.-D.; Tai, H.-L. A chitosan/amido-graphene oxide-based self-powered humidity sensor enabled by triboelectric effect. *Rare Met.* **2021**, *40*, 1995−2003.
(41) Zhou, Y. S.; Wang, S.; Yang, Y.; Zhu, G.; Niu, S.; Lin, Z.-H.; Liu, Y.; Wang, Z. L. Manipulating nanoscale contact electrification by an applied electric field. *Nano Lett.* **2014**, *14* (3), 1567−1572.
(42) Xu, C.; Zi, Y.; Wang, A. C.; Zou, H.; Dai, Y.; He, X.; Wang, P.; Wang, Y.-C.; Feng, P.; Li, D.; Wang, Z. L. On the Electron-Transfer Mechanism in the Contact-Electrification Effect. *Adv. Mater.* **2018**, *30* (15), 1706790.
(43) Zhang, S. L.; Xu, M.; Zhang, C.; Wang, Y.-C.; Zou, H.; He, X.; Wang, Z.; Wang, Z. L. Rationally designed sea snake structure based triboelectric nanogenerators for effectively and efficiently harvesting ocean wave energy with minimized water screening effect. *Nano Energy* **2018**, *48*, 421−429.
(44) Liang, X.; Jiang, T.; Liu, G.; Feng, Y.; Zhang, C.; Wang, Z. L. Spherical triboelectric nanogenerator integrated with power management module for harvesting multidirectional water wave energy. *Energy Environ. Sci.* **2020**, *13* (1), 277−285.
(45) Xu, M.; Zhao, T.; Wang, C.; Zhang, S. L.; Li, Z.; Pan, X.; Wang, Z. L. High Power Density Tower-like Triboelectric Nanogenerator for Harvesting Arbitrary Directional Water Wave Energy. *ACS Nano* **2019**, *13* (2), 1932−1939.
(46) Xu, L.; Pang, Y.; Zhang, C.; Jiang, T.; Chen, X.; Luo, J.; Tang, W.; Cao, X.; Wang, Z. L. Integrated triboelectric nanogenerator array based on air-driven membrane structures for water wave energy harvesting. *Nano Energy* **2017**, *31*, 351−358.

https://doi.org/10.1021/acsenergylett.1c01092
ACS Energy Lett. 2021, 6, 2809−2816